Robust Surface Warming in Offshore China Seas and Its Relationship to the East Asian Monsoon Wind Field and Ocean Forcing on Interdecadal Time Scales

RONGSHUO CAI

Key Laboratory of Global Change and Marine-Atmospheric Chemistry, Third Institute of Oceanography, State Oceanic Administration, Xiamen, China

HONGJIAN TAN

Key Laboratory of Global Change and Marine-Atmospheric Chemistry, Third Institute of Oceanography, State Oceanic Administration, Xiamen, and State Key Laboratory of Atmospheric Sciences and Geophysical Fluid Dynamics, Institute of Atmospheric Physics, Chinese Academy of Sciences, Beijing, China

HARILAOS KONTOYIANNIS

Hellenic Center for Marine Research, Attica, Greece

(Manuscript received 18 December 2015, in final form 1 August 2017)

ABSTRACT

Robust surface warming with distinct interdecadal variations has been observed in the offshore area of China and adjacent seas (hereafter, offshore China) during winter and summer of the period 1958–2014. Acceleration of this warming during 1980–99 at rates greater than the global mean warming rate was accompanied by a weakening of the East Asian monsoon (EAM) and a strengthening of the west Pacific subtropical high (WPSH). It was determined that the sea surface temperature (SST) variation in offshore China correlates very well with changes in the EAM wind on interdecadal time scales. It was also established that the enhanced oceanic lateral heat transfer, mainly attributed to the leading empirical orthogonal function (EOF1), weakening EAM wind mode, has a central role in robust interdecadal winter surface warming in offshore China. However, except for the effect of oceanic lateral heat transfer, the increased surface heat flux through radiative heating related to the third EOF (EOF3) strengthening EAM anticyclone wind mode (WPSH) in summer appears to have a greater contribution to interdecadal summer surface warming in offshore China. These results help clarify the relationship between interdecadal SST variations, EAM, oceanic currents, and sea surface flux in offshore China.

1. Introduction

Warming of the upper ocean over recent decades has been firmly established for almost all latitudes and oceans, including the Pacific and its marginal seas, although estimates of the warming rate vary (Trenberth et al. 2007; Rhein et al. 2013; Hoegh-Guldberg et al. 2014; Cai et al. 2016). Sea surface temperature (SST) has increased synchronously with ocean warming in the offshore area of China and adjacent waters of the marginal seas in the northwestern Pacific Ocean, especially in shallow areas (hereafter referred to as offshore China) (Hoegh-Guldberg et al. 2014; Cai et al. 2016). The observed rapid warming in offshore China has been robust and persistent on interdecadal time scales since the late 1970s, although its characteristics have varied with location. For example, areas of obvious warming have appeared in the East China Sea (ECS) and adjacent seas in winter [December–February (DJF)], and in the northern ECS, Yellow Sea (YS), and Japan–East Sea in summer [June–August (JJA)] (Cai et al. 2011). Rates of SST increase in offshore China and adjacent seas [e.g., 0.279°C decade^{-1} in the YS, 0.4°C decade^{-1} during winter in the YS–ECS, and 0.16°C decade^{-1} in the central South China Sea (SCS)] (Cai et al. 2009; Sherman et al. 2009; Yeh and Kim 2010), are higher than global and large-scale regional warming trends (Rhein et al. 2013).

Corresponding author: Rongshuo Cai, rscai@163.com

DOI: 10.1175/JCLI-D-16-0016.1

Since the late 1970s, persistent surface warming in offshore China has been accompanied by a weakening of the East Asian monsoon (EAM) wind (Cai et al. 2011; Yeh and Kim 2010). Zhang et al. (2012) indicated that wind anomalies over the Kuroshio (KC) area were responsible for decadal KC heat transport variations and contributed to interdecadal SST variations in the ECS (Qi et al. 2010). Oey et al. (2013) observed that coastal wintertime [January–March (JFM)] warming in eastern offshore China since 1998 was accompanied by a stronger northeasterly monsoon wind. These observations seem to indicate the existence of different mechanisms connecting SSTs and wind anomalies. Therefore, we are trying to better understand whether there are different relationships between long-term SST variations and EAM wind across offshore China, and if so, what mechanisms are involved in these relationships. According to Bjerknes (1964), most short-term SST variability over the midlatitude North Atlantic is driven directly by the atmosphere on interannual time scales. Moreover, the Atlantic Ocean itself contributes to multidecadal control of surface heat fluxes (Gulev et al. 2013). Until now, however, there has been no investigation of long-term interdecadal variations of SST in offshore China and its relationship to atmospheric and oceanic forcing, nor whether these long-term SST changes in recent decades have been driven mainly by lateral oceanic heat transfer or are affected directly by atmospheric wind and radiative forcing.

Summer surface warming in eastern offshore China can be attributed to solar shortwave heating that preferentially affects the upper-ocean layer above the seasonal pycnocline (Belkin 2009). Atmospheric radiation over offshore China is closely linked to changes in the west Pacific subtropical high (WPSH) and concentrations of marine aerosols and greenhouse gases. The WPSH, which is the primary subtropical anticyclone over the North Pacific and offshore China, can greatly influence the interannual relationship between SST and the monsoon (Chang et al. 2000). Cai et al. (2009) suggested that sea surface warming in the SCS on interannual time scales is linked to westward extension of the WPSH, which has persisted since the 1980s (Zhou et al. 2009). The changes in EAM wind and WPSH, and the increase in aerosols and other air pollutants can profoundly impact SST by altering atmospheric radiative heating, water vapor convergence, and rainfall patterns in eastern China (Zhu et al. 2012). Nevertheless, the relationship between long-term interdecadal SST changes in offshore China and surface heat flux (which is related to changes in EAM wind, the WPSH, and atmospheric radiation) remains poorly understood. Long-term variations of sea surface heat flux, including longwave radiation (LW), shortwave radiation (SW), sensible heat (SH), and latent heat (LH), and their roles in coastal warming at interdecadal time scales also remain unclear.

The objective of this study is to investigate the interdecadal SST variation in offshore China and its response to long-term atmospheric and oceanic forcing mechanisms, including changes in EAM wind, ocean currents, surface heat flux, and their interrelationships. The remainder of the paper is organized as follows. First, we examine interdecadal variability of SST in offshore China and EAM wind in winter and summer for 1958–2014, which is a much longer period than considered in earlier studies (Cai et al. 2011; Yeh and Kim 2010; Oey et al. 2013). Second, we investigate the relationships and mechanisms between interdecadal SST changes in offshore China, EAM lower atmospheric circulations, and ocean currents. Third, we examine the interdecadal variability of the WPSH and sea surface heat flux, oceanic advection, and their relationship to SST and EAM wind changes in offshore China. Finally, the interdecadal SST variations related to EAM wind and oceanic forcing in that region are summarized.

2. Data and methods

The 1° × 1° Hadley Centre Sea Ice and Sea Surface Temperature monthly dataset (HadISST) for 1958–2014 (Rayner et al. 2003) is used to investigate linear trends and interdecadal variations of SST. The 1.25° × 1.25° Japanese 55-year Reanalysis Project (JRA-55) monthly dataset for 1958–2014 (Ebita et al. 2011) is used to examine interdecadal variations of EAM wind in winter and summer. The Simple Ocean Data Assimilation (SODA, version 2.1.6) dataset of monthly current velocities on a 0.5° × 0.5° grid (Carton and Giese 2008) is also used, from which flows at depths of 5, 15, 25, 35, and 45 m are considered for 1958–2008 (period of data availability) to derive long-term variations in upper mean ocean currents. The 1° × 1° objectively analyzed air–sea fluxes (OAFlux; http://oaflux.whoi.edu/data.html) monthly dataset for 1958–2014, including SH and LH and the 1° × 1° International Satellite Cloud Climatology Project (ISCCP) monthly dataset (http://isccp.giss.nasa.gov/projects/flux.html) for net surface SW radiation (positive downward) and net surface LW radiation (positive upward) from July 1983 to December 2009 (period of data availability), are used to estimate changes of sea surface heat flux during 1984–2009. The net atmospheric radiation is referred to as the net surface SW minus the net surface LW over offshore China.

Several WPSH indices such as area, intensity, and westward extension during 1958–2014, released by the Chinese National Climate Center and widely used in previous studies (e.g., Mu et al. 2001), along with net shortwave solar radiation ($W\,m^{-2}$) data from the National Centers for Environmental Prediction–National

Center for Atmospheric Research (NCEP–NCAR) for 1958–2014, with a horizontal resolution of 2.5° × 2.5° (Kalnay et al. 1996), are used to describe WPSH activity and its relationship with shortwave solar radiation for 1958–2014. The three WPSH indices are defined as follows: 1) the area index is represented by the area-weighted sum of the number of grid points in the region enclosed by the 588-dgpm contour at 500 hPa; 2) the intensity index is defined using geopotential height values at grid points inside the same area; and 3) the westward extension index is the most westerly longitude reached by the 588-dgpm contour, representing the longitude of the western edge of the WPSH ridge.

Statistical methods such as linear trend analysis, conventional empirical orthogonal function (EOF) and multivariate EOF (MV-EOF) (e.g., Wang 1992), multiple linear regression, and correlation analysis are performed. Long-term spatiotemporal variations of SST and EAM wind (velocity in zonal and meridional components at 925 hPa) over offshore China are investigated using conventional EOF and MV-EOF analyses, respectively. To identify interdecadal variation features of SST and EAM wind during 1958–2014, their respective time series were first decomposed into long-term interdecadal and secular components by 8-yr low-pass filtering, using the appropriate Lanczos filters (Duchon 1979). However, we mainly consider interdecadal variability of the 8-yr low-pass-filtered records, in which the contained secular components are removed.

Unless otherwise indicated, the presented EOF and MV-EOF analysis results refer to those EOFs that account for >15% of the total variance, while the absolute values of the correlation coefficients between EOF time coefficients [principal components (PCs)] of the corresponding EAM and SST are >0.45, and their correlations are based on the 95% confidence level. The statistical confidence level is estimated using the Student's t test with $(N-2)$ degrees of freedom. However, because we use the 8-yr low-pass-filtered time series, the actual "effective" degrees of freedom (N_{eff}) used are estimated by $N_{\text{eff}} = (r_1/r_2)(N-2)$, where r_1 and r_2 are autocorrelation coefficients of two filtered variables (Trenberth 1984). Hereafter, the significance testing of the filtered data follows the newly established N_{eff}, unless otherwise stated.

3. Results and discussion

a. Variation of SST in offshore China

Figure 1 shows the magnitudes of long-term, spatial linear SST changes for the global ocean, including offshore China (0°–45°N, 100°–140°E), during 1958–2014. Winter SSTs during 1958–2014 in the ECS (23°–40°N, 120°–130°E, including the Bohai Sea, YS, and ECS) and SCS (2°–23°N, 110°–120°E) regions increased by 1.71° ± 0.23°C (at a rate of 0.3° ± 0.04°C decade^{-1}) and 1.02° ± 0.17°C (at a rate of 0.18° ± 0.03°C decade^{-1}), respectively (Figs. 1a and 1c). Corresponding increases in summer were 0.86° ± 0.17°C (at a rate of 0.15° ± 0.03°C decade^{-1}) and 0.74° ± 0.11°C (at a rate of 0.13° ± 0.02°C decade^{-1}) (Figs. 1b and 1d) for 1958–2014. Figures 1e and 1f present the time series of average SST anomalies for the global ocean, Northern Hemisphere oceans, and ECS and SCS regions during winter and summer 1958–2014. The acceleration of offshore China warming since the late 1970s is greater than both the total value and rate of global upper 75-m ocean warming of 0.11° ± 0.02°C decade^{-1} for 1971–2010 (Rhein et al. 2013).

The analyzed magnitude of SST increase for offshore China (Fig. 1) [i.e., 0.83° ± 0.02°C at a rate of 0.15°C decade^{-1} for 1958–2014; Cai et al. (2016)], is similar to the increase of 1.2°C reported for the annual mean SST in the northeastern ECS and Japan Sea during 1900–2002 (Tian et al. 2012), and Korean waters over the past 40 years (Jung et al. 2014). The magnitude of surface warming in offshore China is greater than the 1.1°C increase during 1950–2008 observed in the KC area, attributed to the intensification of meridional heat transport from the tropical Pacific Ocean (Wu et al. 2012). The KC usually intrudes into the ECS from both sides of the Taiwan Island and the northern SCS through the Luzon Strait (Chao 1991). It is plausible that accelerated surface warming in offshore China could result from the influence of the KC, in addition to long-term changes in atmospheric circulation such as the EAM wind, WPSH, and related atmospheric forcings, which impact the ocean on time scales of >10 yr (Cai et al. 2009, 2011; Zhang et al. 2012; Oey et al. 2013). Aside from the KC branch, SST in offshore China can be affected by the Taiwan Warm Current (TWC), the Yellow Sea Warm Current (YSWC), the Yellow Sea Coastal Current (YSCC), and the Zhejiang–Fujian Coastal Current (ZFCC), which are southward coastal cold flows from the YS to the southern ECS and the Taiwan Strait (Zheng et al. 2006).

Figures 2a and 2b show the climatological mean SST in offshore China during winter and summer 1981–2010, which is superimposed on the climatological mean EAM wind during the same period. The leading EOFs (EOF1s) of SST anomalies for winter and summer during 1958–2014 are shown in Figs. 2c–f together with their PC1s. The EOF1 SST anomalies explain 54.4% and 47.1% of the total variance during winter and summer, respectively. The SST in offshore China exhibits a spatial in-phase warming, which is stronger from the ECS to south of the Taiwan Strait during winter (Figs. 2c and 2e) and stronger in the YS, northern ECS, and Japan–East Sea during

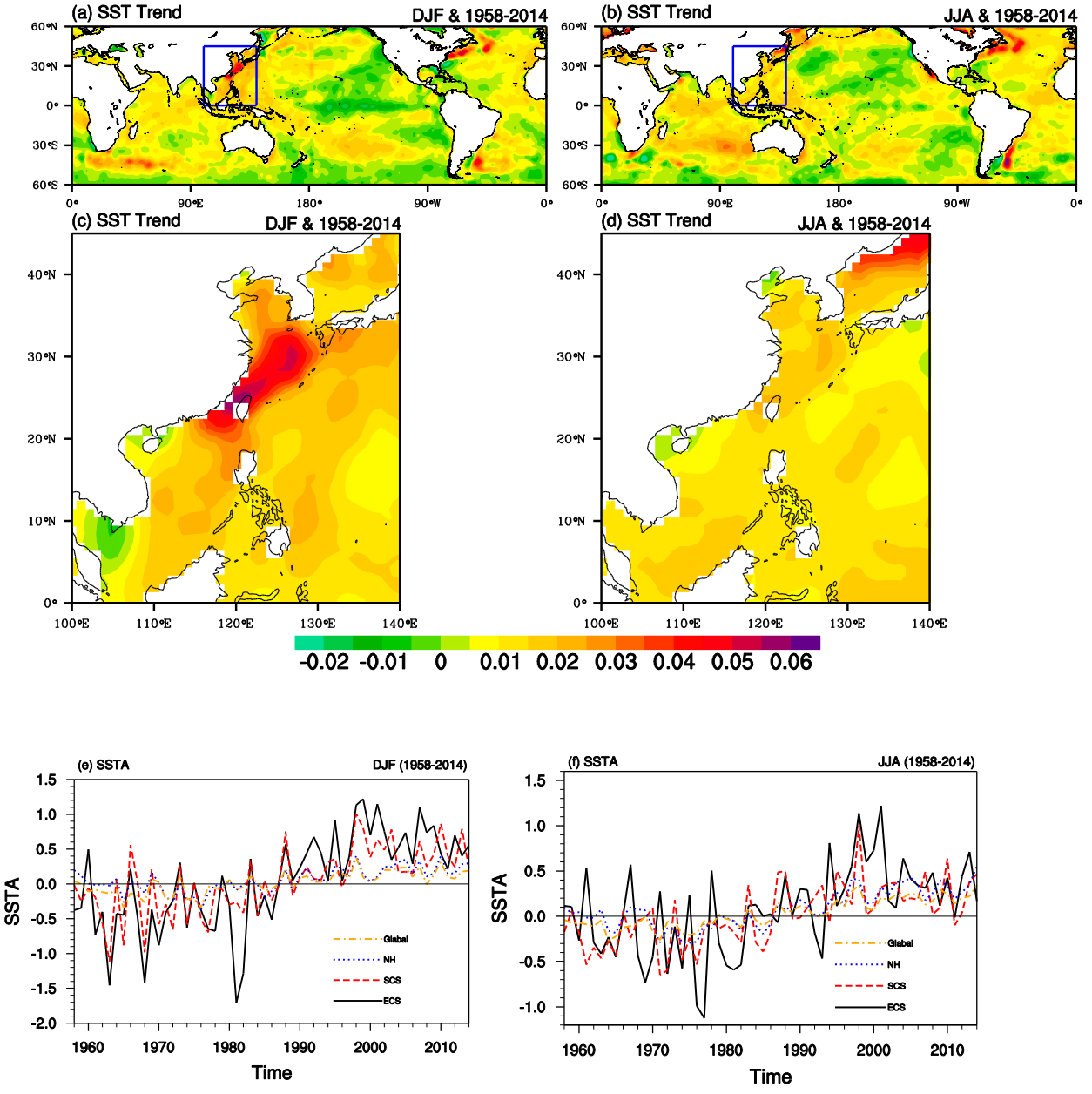

FIG. 1. Spatial patterns of linear sea surface temperature (SST, °C) changes in (a),(b) the global ocean and (c),(d) the offshore area of China and adjacent seas in (a),(c) winter and (b),(d) summer during 1958–2014, along with (e),(f) the time series of average SST anomalies in the global ocean (brown dot–dashed line), Northern Hemisphere oceans (blue dotted line), East China Sea (black solid line), and South China Sea (red dashed line) in (e) winter and (f) summer for the same period. Data are from HadISST reanalysis datasets.

summer (Figs. 2d and 2f). The PC1s (SST) show substantial interannual and interdecadal SST variations, with a warming regime shift around the late 1970s and a hiatus after 1999. Therefore, the relevant variations and relationships of SST and EAM wind are analyzed, with a focus on interdecadal time scales after appropriate low-pass filtering of SST and EAM wind time series using Lanczos filters (Duchon 1979).

b. Relationships of interdecadal SST variations in offshore China to EAM wind and upper-ocean currents

1) WINTER

The EOF1s of the interdecadal winter SST variations in offshore China and of the East Asian winter monsoon

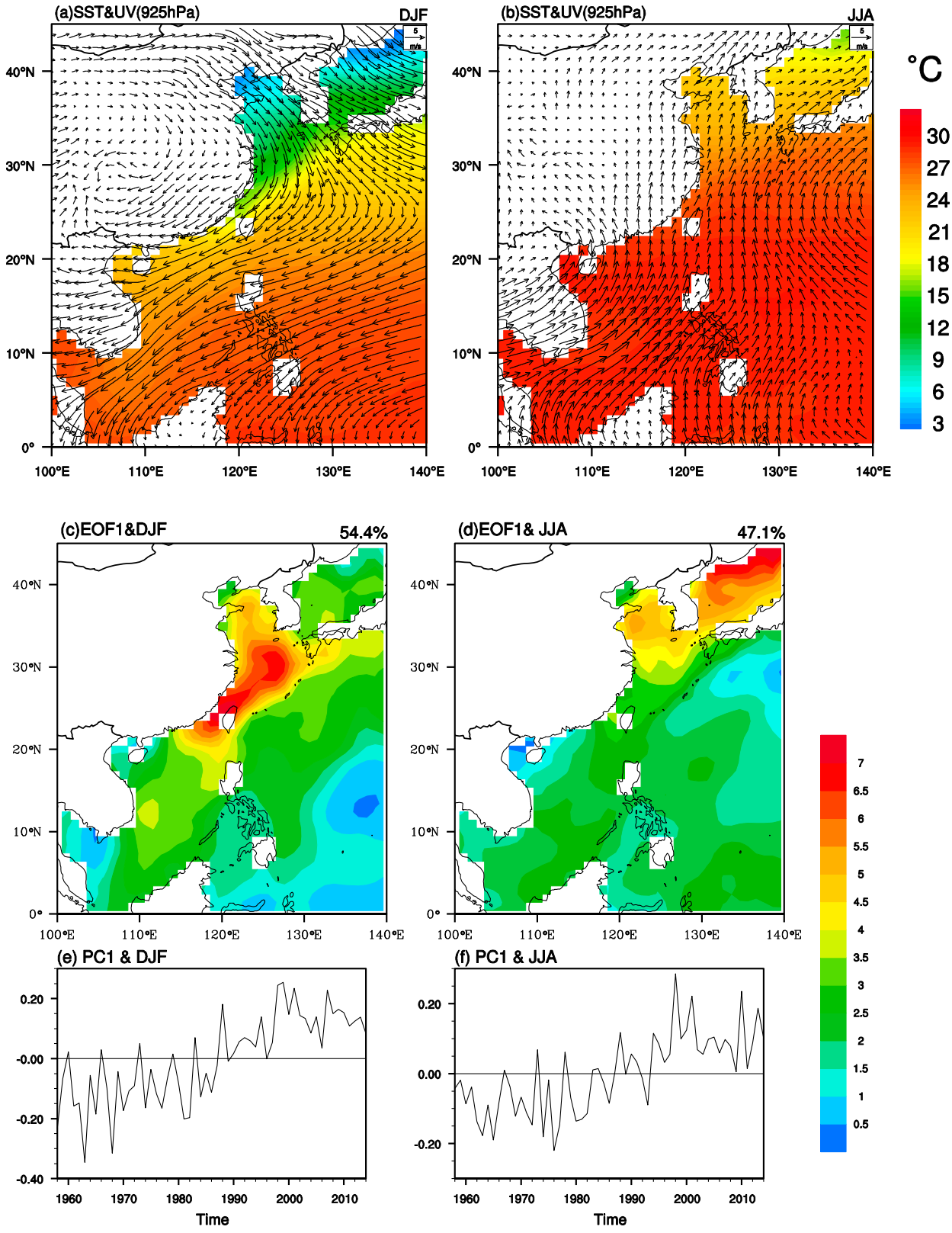

FIG. 2. Climatological mean wind fields [black vectors, reference vector in the top right corner of (a),(b) in m s^{-1}] at 925 hPa and mean SST (color shading, °C) for (a) winter and (b) summer during 1981–2010 along with spatial patterns of (c),(d) SSTAs and (e),(f) time coefficients (PC1s) for the leading empirical orthogonal function mode (EOF1) during (c),(e) winter and (d),(f) summer for 1958–2014. Data are from HadISST and JRA-55.

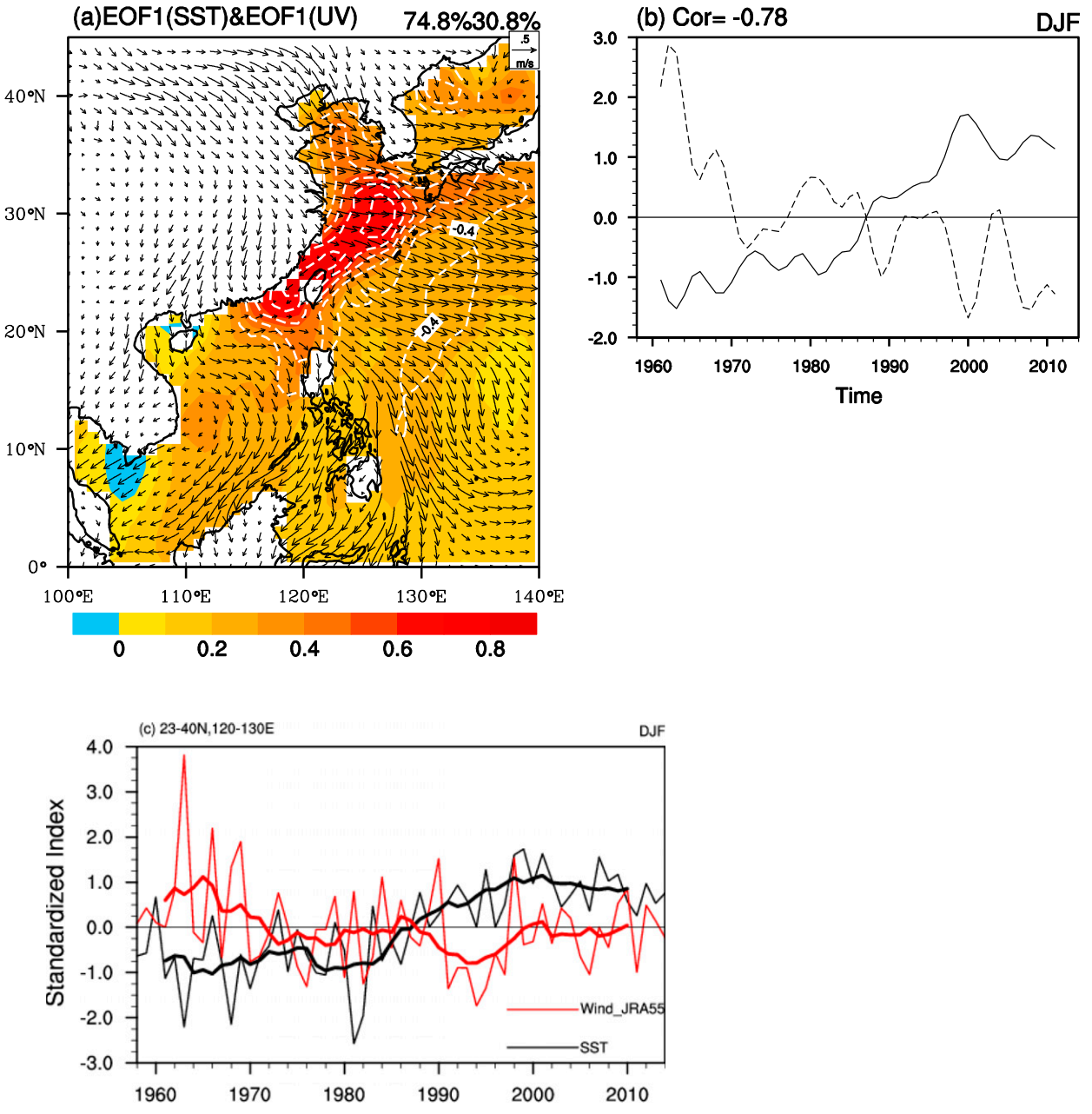

FIG. 3. (a) Spatial patterns and (b) time coefficients (PCs) of the leading empirical orthogonal function mode (EOF1) for the 8-yr, low-pass-filtered winter SST anomaly (color shading) and East Asian winter monsoon (EAWM) wind field at 925 hPa [black vectors, reference vector in the top right corner of (a) in m s^{-1}] along with the time series (c) of EAWM wind velocity indices (red) and SST (black) over the East China Sea. The thin (thick) line in (c) indicates the time series of indices in seasonal mean (5-yr running mean). The solid (dashed) line in (b) represents the time series of the principal component (PC1) for the SST anomaly (wind field). The white dashed contours in (a) represent the spatial pattern of regressed SST against the PC1 of the wind field; values range from −0.4 to −0.9 at intervals of 0.1 (only shown at 95% confidence level). Data are from HadISST and JRA-55.

(EAWM) wind (Figs. 3a and 3b) explain 74.8% and 30.8% of the total SST and wind variance, respectively. The EOF1s of SST and EAWM mainly display variation patterns of in-phase SST and southward meridional winds (Fig. 3a), whereas the correlation coefficient (CC) of the PC1 (SST) and PC1 (EAWM) is −0.78 (Fig. 3b). Robust interdecadal surface warming has occurred in the region from the ECS shelf to the southern Taiwan Strait (Figs. 3a,b), where the coefficients of the SST regression against the PC1 of the EOF1 EAWM wind range from −0.4 to −0.9 at the 95% confidence level (Fig. 3a).

TABLE 1. Correlation coefficients between PCs of SST and EAWM for 1958–2014.

Epoch	8-yr low-pass filtering	Detrended PC1 time series
1958–79	−0.85	−0.61
1980–98	−0.85	−0.69
1999–2014	−0.64	−0.85

However, there is a question as to whether the large CC of PC1 (SST) and PC1 (EAWM) (Fig. 3b) may be elevated because of a secular trend or different time scales. After both time series of PC1s for 1958–2014 were detrended, the CC declined from −0.78 to −0.1, which indicates that the high correlation between SST-PC1 and EAWM-PC1 is linked to the secular trend during 1958–2014. After a steady period during the middle twentieth century, SST in offshore China increased rapidly during 1980–99, followed by a hiatus after 1999 (Figs. 1e,f and 3c), with a slightly reamplified EAWM in the mid-2000s, which is similar to the results of Wang and Chen (2014). For this reason, the entire 1958–2014 period was divided into three epochs (1958–79, 1980–98, and 1999–2014), and the corresponding CCs were estimated after removing trends (Table 1). The results indicate that the large CC of the PC1s of SST and EAWM (Table 1) is also closely linked to decadal and bidecadal changes. Therefore, the role that EAM plays in the robust interdecadal warming will be investigated in the following sections.

Our findings suggest that there is a link between interdecadal warming of the winter SST in offshore China and weakening of the northerly EAWM wind. In our case, the dominant winter wind direction appearing in the EOF1 (Fig. 3a) is mostly from the northwest, while in the Taiwan Strait it is from the northeast. These are the same wind directions found by Cai et al. (2011) and are consistent with the results of Oey et al. (2013), who reported an increase in northeasterly wind over the Taiwan Strait after 1997–98, which favors heat transport from the KC into the coastal China Sea. Oey et al. (2013) also reported a parallel weakening of the EAWM over central and eastern China. However, both studies are in near-qualitative agreement with respect to favoring intrusion of the KC and TWC into the southern ECS shelf area. Oey et al. (2013, 2014) suggested that strong northeasterly monsoon relaxation since 1998 would favor more frequent across-shelf intrusions and cross-strait currents from the warm KC and TWC.

The following describes a possible mechanism for the observed link between winter SST and EAWM. Because of wind-driven Ekman advection (Chang et al. 2010; Chao 1991), the southward upper Ekman drift current associated with weakening northwesterly winds occurs in a direction close to that of the wind (nearly 90°), and favors northward advection of the KC and its cross-shelf

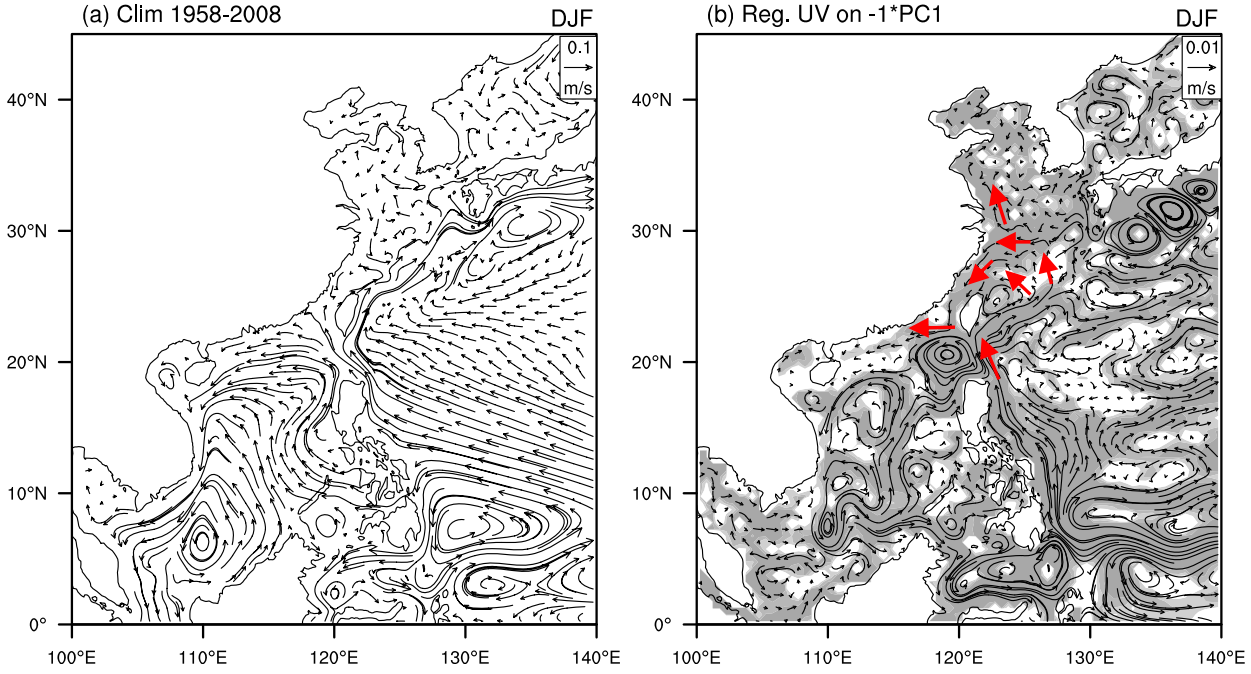

FIG. 4. (a) Distributions of winter climatological mean upper 30-m ocean currents in offshore China for 1958–2008. (b) Spatial patterns of the 8-yr, low-pass-filtered winter upper-ocean current regression with −1 × PC1 of the East Asian winter monsoon (EAWM) wind field at 925 hPa for 1958–2008 (shaded areas exceed 95% confidence level). Reference vectors are in the top right corner of (a),(b) in m s^{-1}. Data are from SODA dataset and JRA-55.

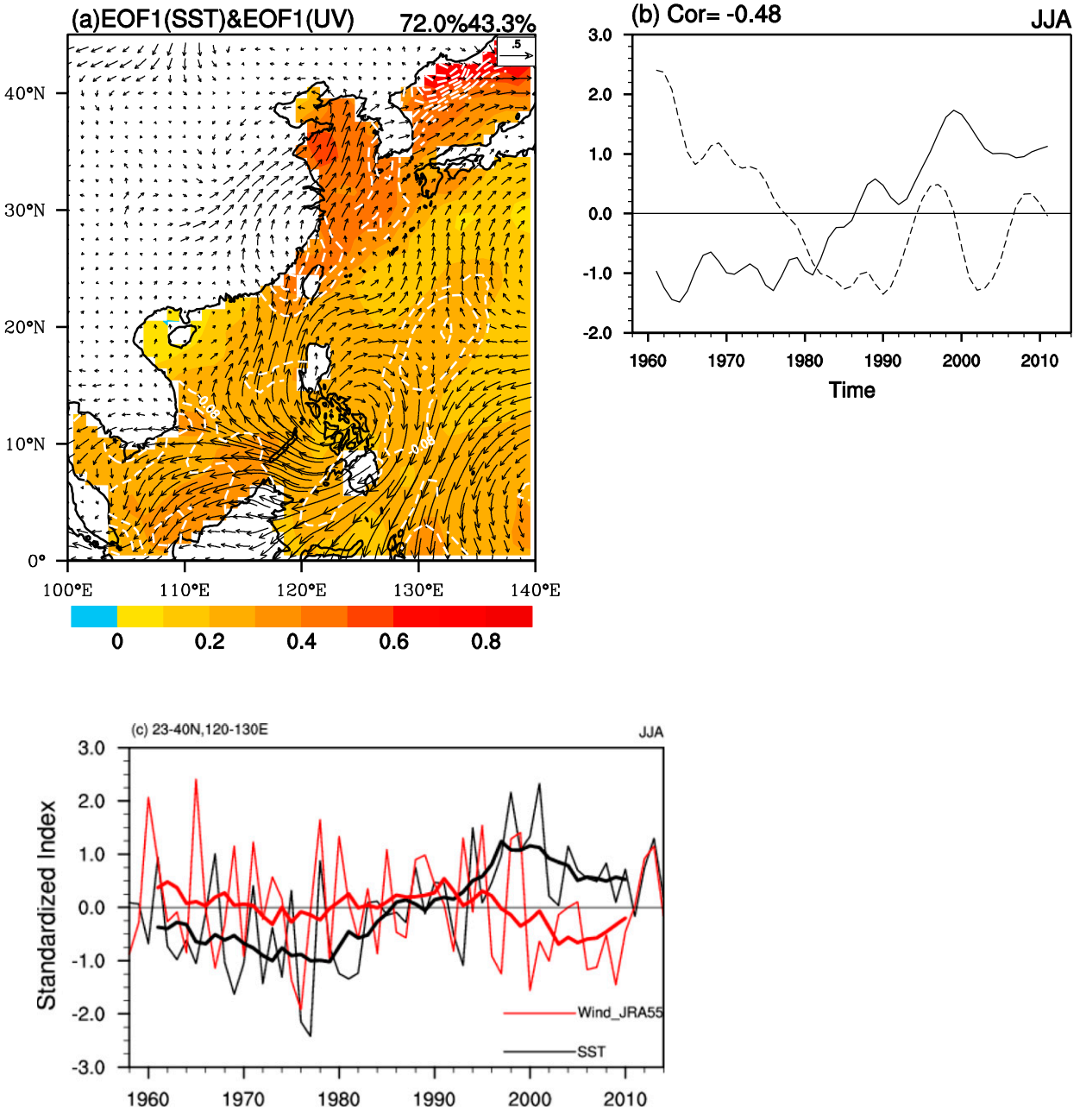

FIG. 5. As in Fig. 3, but for summer and with white contours in (a) ranging from −0.2 to −0.5 at intervals of 0.05 and with data from HadISST and JRA-55.

currents into the ECS. On the other hand, strengthening northwesterly winds after 1999 shown in Figs. 3a and 3b would weaken northward advection of the KC and its cross-shelf currents into the ECS due to strong southward upper Ekman drift. Moreover, weakening (strengthening) northeasterly winds over the Taiwan Strait before (after) 1999 would favor (not favor) poleward flow of the warm TWC into the ECS (Chao 1991; Oey et al. 2014).

Figure 4a shows the climatological winter mean ocean current in the upper 30-m layer of offshore China (e.g., Zheng et al. 2006). The spatial pattern of the upper 30-m current velocity regression against the PC1 (EAWM) is shown in Fig. 4b, in which the shaded areas correspond to significant negative correlations (e.g., surrounding the current in the YS, the northern and offshore ECS, the KC area, and west of the Luzon Strait). This indicates that a weakening (strengthening) of the southward

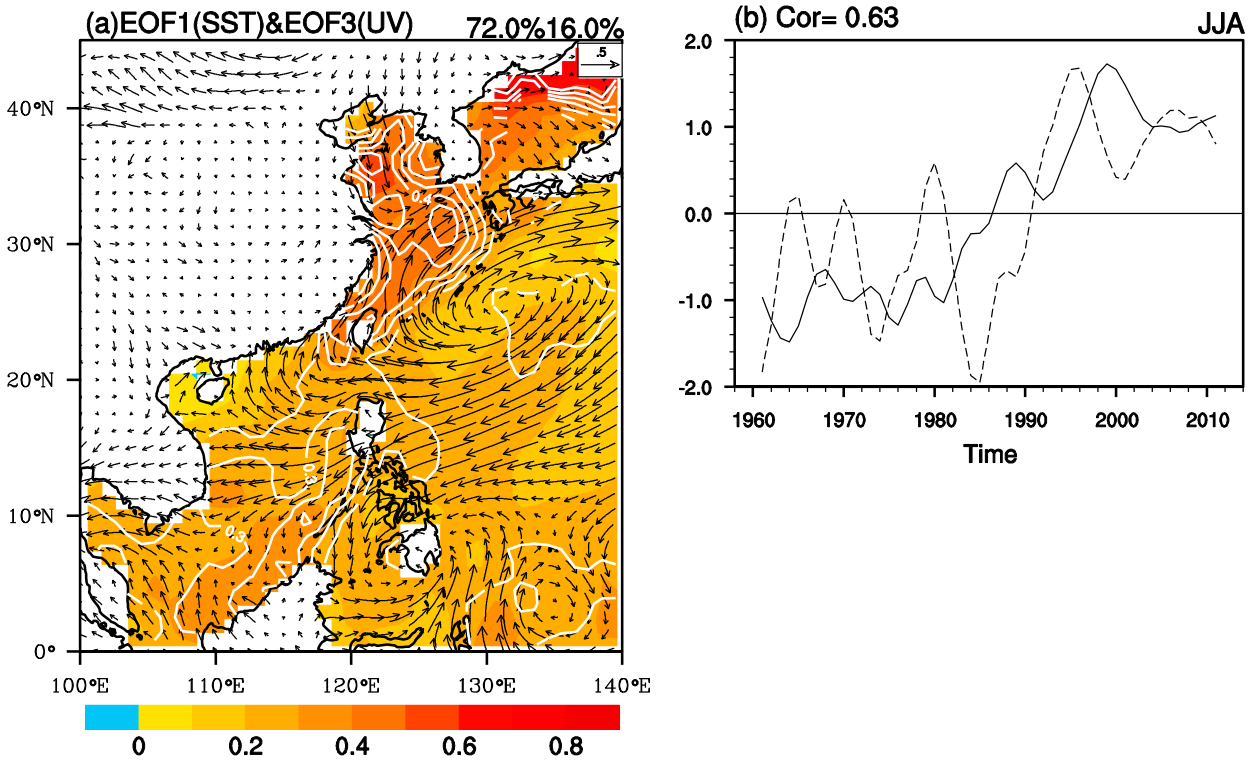

FIG. 6. (a),(b) As in Fig. 3, but for the third EOF (EOF3) of the EASM wind field at 925 hPa and with the solid (dashed) line in (b) representing the time series of the principal component PC1 (PC3) for the SST (EASM) anomaly and the white contours in (a) showing the spatial pattern of the regressed SST with PC3 of the wind field, ranging from 0.25 to 0.65 at intervals of 0.05.

YSCC from the YS and northern ECS and a strengthening (weakening) warm KC flowing toward the ECS and Taiwan Strait and into the SCS through the Luzon Strait passively responds to an interdecadal weakening (strengthening) EOF1 EAWM wind, which was also demonstrated by Cai et al. (2015, see their Fig. 6a). Qualitatively, this ocean heating process driven by ocean dynamics on interdecadal time scales is similar to that of the midlatitude Atlantic Ocean on longer time scales shown by Gulev et al. (2013).

2) SUMMER

EOF1's in-phase spatial structures of the summer SST and East Asian summer monsoon (EASM) wind are shown in Figs. 5a and 5b, together with their PC1 time series. They explain 72.0% and 43.3% of the total summer SST and EASM variance, respectively. The correlation of PC1s of the SST and EASM wind is −0.48 (Fig. 5b). This indicates that significant surface warming occurs in the ECS, YS, and Japan–East Sea with a weakening EASM after the 1980s (Fig. 5b), as well as a similar decadal shift of EASM to that observed by Zhang (2015). Superimposed on Fig. 5a are the white dashed contours of the summer SST regression against the PC1 of the EOF1 EASM wind. The negative correlation areas indicate that the weakening EOF1 EASM wind, which occurred after the 1980s (Fig. 5), corresponds to surface coastal warming, particularly from south of the Taiwan Strait to the Japan–East Sea. A summer hiatus in surface warming occurs after 1999, in parallel with relaxation of the EASM wind (Fig. 5c).

In contrast to the wind EOF variance decomposition in winter, there are two dominant EOF EASM wind modes—those of the EOF1 northward meridional wind and EOF3 anticyclonic circulation—which closely correlate with SSTs on interdecadal time scales (Fig. 6). The EOF3 EASM wind explains 16.0% of the total summer wind variance. The PC1 (SST) correlates positively with the PC3 (EASM), with a CC of 0.63 (Fig. 6b). The EOF3 EASM depicts a large-scale anticyclone that stretches across the northwest Pacific and offshore China, which reflects the typical pattern of the WPSH. This anticyclone has been extending westward with some oscillations since the mid-1980s (Fig. 6b), which is similar to the findings of Zhou et al. (2009).

Figure 6a displays the spatial pattern of summer SST regression against the PC3 (EASM). The regression coefficients are positive and range from 0.25 to 0.65. This indicates that changes in SST over the ECS, YS, and Japan–East Sea show a greater response to the EOF3

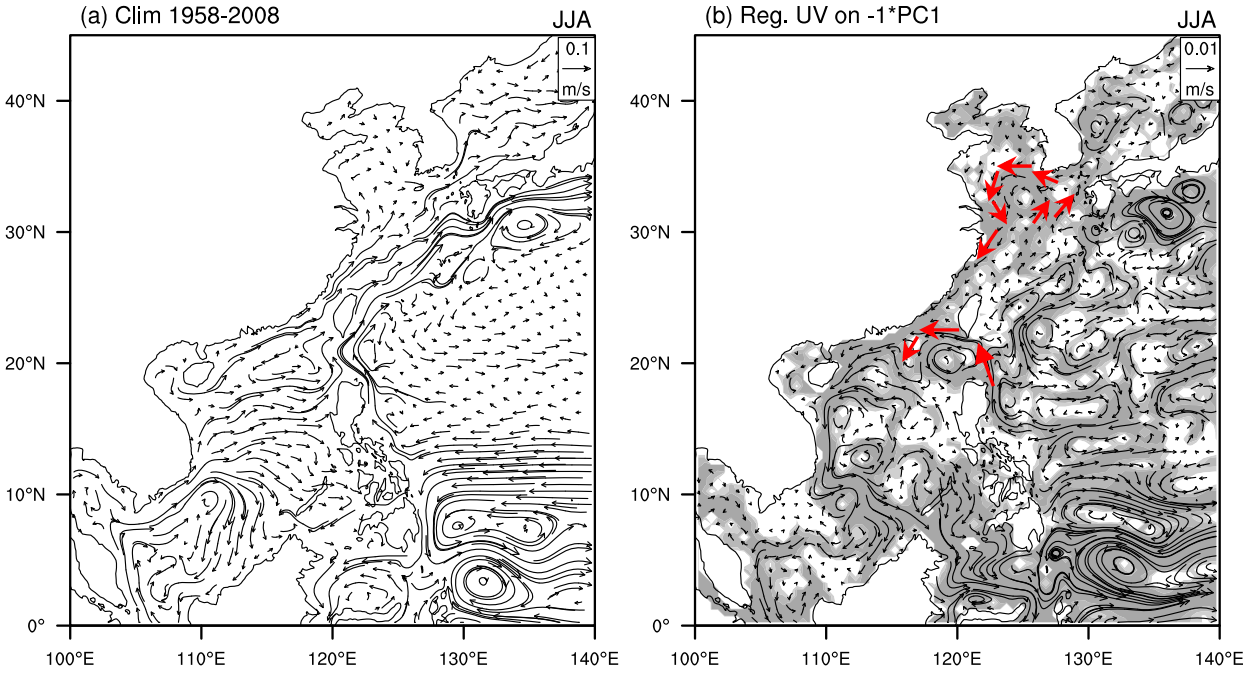

FIG. 7. As in Fig. 4, but for summer.

EASM. The positive regression relationship of SST and PC3 (EASM) implies that sea surface warming in the region was closely associated with a strengthening anticyclone after the mid-1980s.

To identify the relationship between the EOF1 SST and EOF3 EASM modes, CCs of the PC1 (SST) and PC3 (EASM) are examined. The results indicate that the maximum CC is 0.72, with the PC3 (EASM) leading the PC1 (SST) by 2–3 yr for 1984–2014, during which the anticyclone anomaly (WPSH) intensified. Moreover, the maximum CC (0.75) of the PC3 (EASM) leading the PC1 (SST) is much larger than that (−0.45) of the PC1 (SST) leading the PC3 (EASM) for 1958–83. This suggests that the strengthening EOF3 EASM anticyclone wind mode (WPSH) since the mid-1980s has contributed to summer warming in offshore China.

Because of the Ekman effect, strong (weak) eastward and northeastward upper Ekman drift associated with strong (weak) southwesterly and southerly winds over the ECS (Figs. 5a,b) would not (would) favor a KC cross-shelf intrusion into the southern ECS. However, the strong (weak) anticyclone circulation anomalies shown in the EOF3 EASM wind field (Figs. 6a,b) can favor (not favor) the flow of poleward currents in the Taiwan Strait into the southern ECS.

Figure 7a shows the climatological summer upper 30-m ocean currents in offshore China. Figure 7b depicts the spatial pattern of the summer upper 30-m currents regression against the PC1 of the EOF1 EASM. The shading corresponds to the statistically significant correlation between the currents and the PC1 (EASM). The westward branches of the KC into the SCS via the Luzon Strait show a good negative correlation with the PC1 (EASM). In the SCS, the summer cyclonic ocean current structure to the west of the Luzon Strait, characterized by southward flow near the coast of China and a change in direction to the east of the strait, is correlated with the PC1 (EASM). This indicates a cyclonic oceanic flow to the west of the Luzon Strait in response to the weakening EOF1 EASM since the 1980s, and is favorable for westward transport of heat into the northern SCS via the Luzon Strait by the KC.

The YSWC in the southern YS and northeastern ECS increases in cyclonic form with the weakening EASM wind (Fig. 7b), which was also demonstrated by Cai et al. (2015, their Fig. 5a). The change in YSWC occurs because the westward shift of the YSWC is driven by northerly winds, which are generated by the combination of a sea level trough off the China coast and a sea level ridge over the YS (Yuan and Hsueh 2010). This implies that strengthening (weakening) northerly (southerly) winds are favorable for YSWC strengthening, because a weakening EASM northward-directed wind is equivalent to a strengthening anomalous northerly wind. Hence, an increased YSWC, together with a weakening EASM northward-directed wind, can

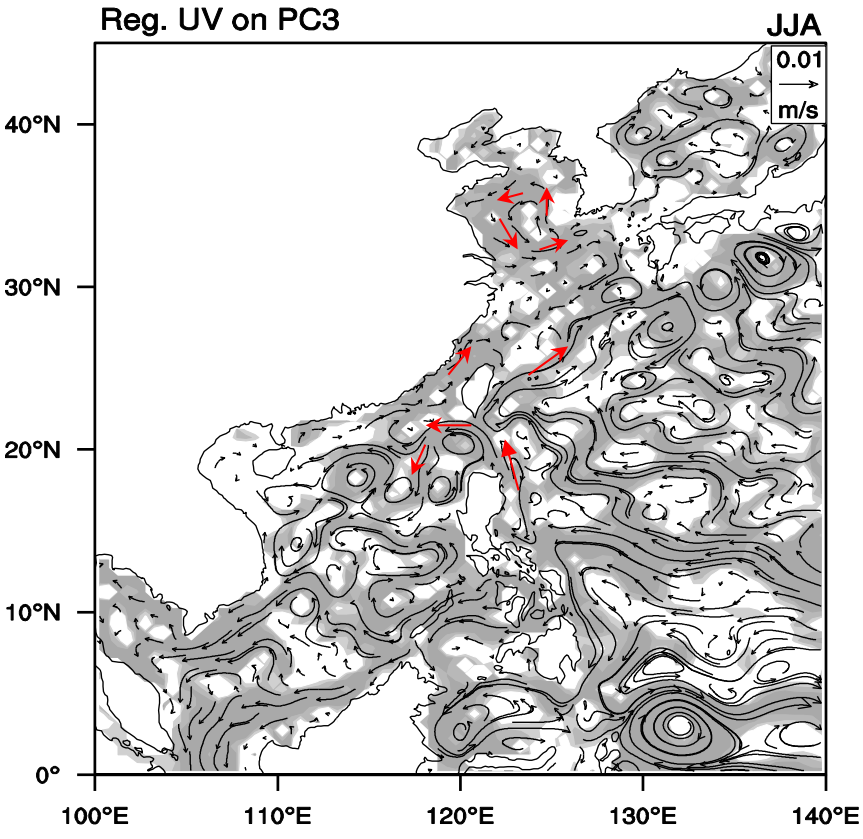

FIG. 8. Spatial pattern of the 8-yr, low-pass-filtered summer upper 30-m ocean current regression with PC3 of the EASM wind field at 925-hPa for 1958–2008. Shaded areas indicate >95% confidence level. Data are from SODA and JRA-55.

favor summer surface warming in the northern ECS and YS (Fig. 6a).

Figure 8 shows the spatial pattern of the summer upper 30-m current regression against the PC3 (EASM). There are three cyclonic currents in the YS, southern ECS, the west Luzon Strait, and northern SCS. These are positively correlated with the EOF3 EASM anticyclone mode. This indicates that the enhanced WPSH is accompanied by an augmentation of both the KC and its inflow branches into the YS, southern ECS, and northern SCS. Similarly, EASM effects on SST can be explained by changes in warm currents such as the YSWC and KC, which are agents of upper-ocean heat transfer.

c. *Relationships between variations of WPSH, surface heat flux, and SST in offshore China*

The WPSH that appears as the EOF3 EASM anticyclone (Fig. 6) can drive ocean heating and support sea surface warming through the downward flux of solar shortwave (SW) radiation. This is generally attributed to reduced cloud coverage within the WPSH area, allowing SW radiation to reach the ocean surface more easily because of the suppression of convective activities (Hu 1997). In contrast, increasing air pollutants and marine aerosols over offshore China can affect SST via changes in SW and LW. Hence, long-term changes of the WPSH and its relationship to SST and SW are examined.

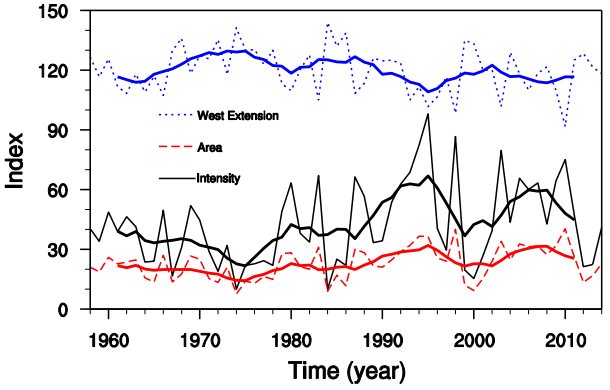

FIG. 9. Long-term changes of summer mean (thin lines) and 8-yr running mean (thick lines) indices of the west Pacific subtropical high (WPSH): area (red), intensity (black), and westward extension (blue) in summer. Data are from the Chinese National Climate Center (CNCC).

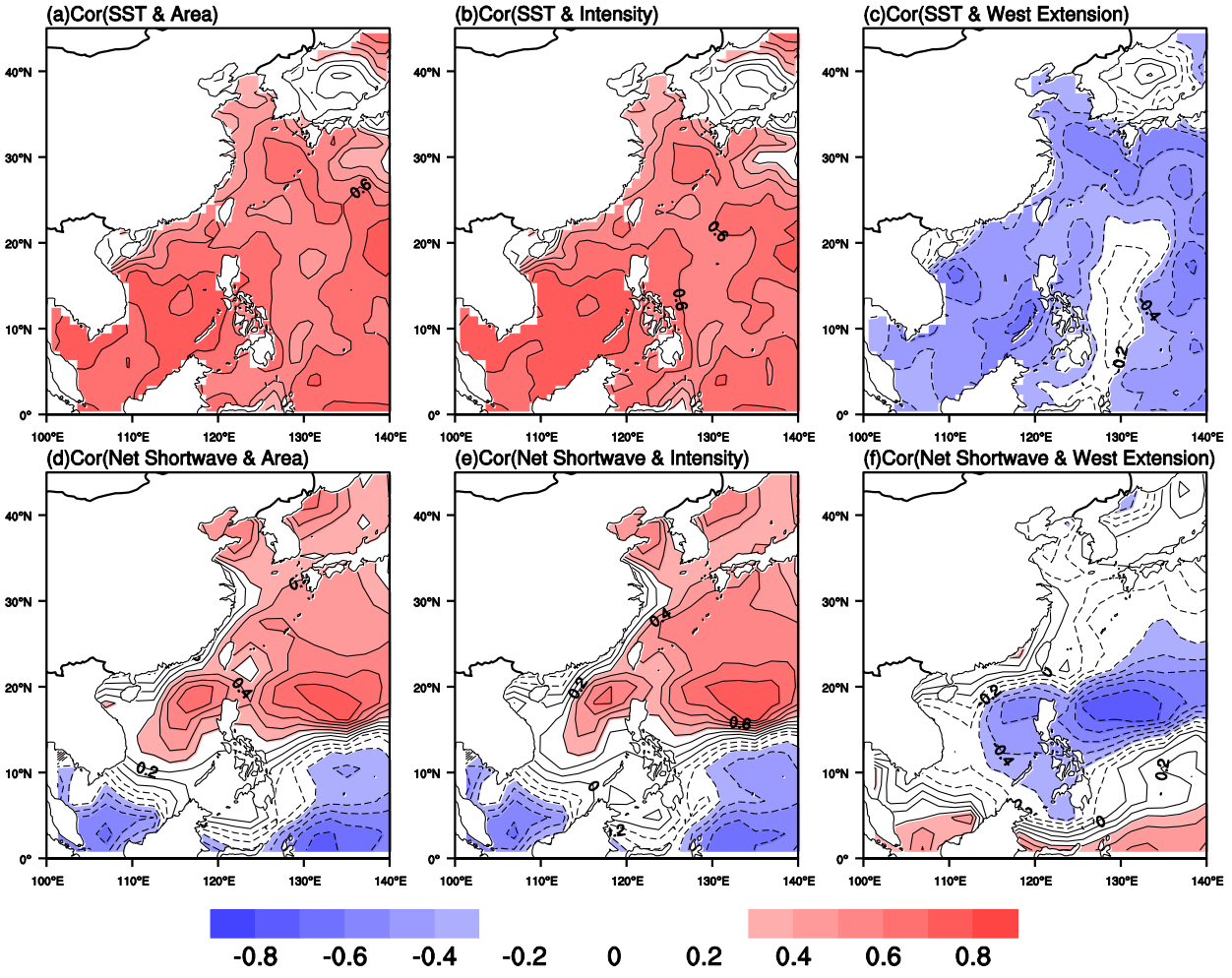

FIG. 10. Spatial patterns of 8-yr, low-pass-filtered correlation coefficients (a)–(c) between SST and WPSH indices and (d)–(f) between shortwave solar radiation and WPSH during summer for 1958–2014: (a),(d) for the area index; (b),(e) for the intensity index; and (c),(f) for the westward extension index. Shading denotes significance at 95% confidence level. Data are from the Chinese National Climate Center, HadISST, and NCEP–NCAR.

Figure 9 indicates that WPSH indices of area and intensity have increased since the late 1970s, in contrast to the westward extension index, which has decreased (owing to the decreasing longitude of the western edge of the WPSH ridge). In fact, the WPSH has strengthened and extended westward since the late 1970s, which is consistent with changes of the anticyclone in summer over the same period (Fig. 6).

Figures 10a–c show the spatial distribution of CCs between the WPSH indices and summer SSTs, while Figs. 10d–f illustrate the significant CCs among the WPSH indices, and summer SW for 1958–2014. The strengthening and westward extension of the WPSH could have contributed considerably to the surface warming in offshore China, which is a similar result to that of Cai et al. (2009). The large CCs of SST and SW for the three WPSH indices, especially in the Bohai Sea, YS, Japan–East Sea, eastern ECS, and northern SCS, indicate that SW heating of the sea surface in offshore China has increased since the 1980s, in parallel with WPSH strengthening.

Given its close proximity to eastern China, the ECS differs from the SCS in its climatological wind fields (Fig. 2) and air–sea exchange. Changes in sea surface heat flux in offshore China are considered separately for the ECS and SCS. Figures 11 and 12 show the time series of net SW, net LW, SH, LH, and total net sea surface heat flux (Q_{net}) during winter and summer for the ECS and SCS during 1984–2009. Positive (negative) values of SW, LW, SH, LH, total net surface heat flux, and net radiation flux (SW − LW) are defined as the ocean receiving (losing) heat from (to) the atmosphere. Therefore, a

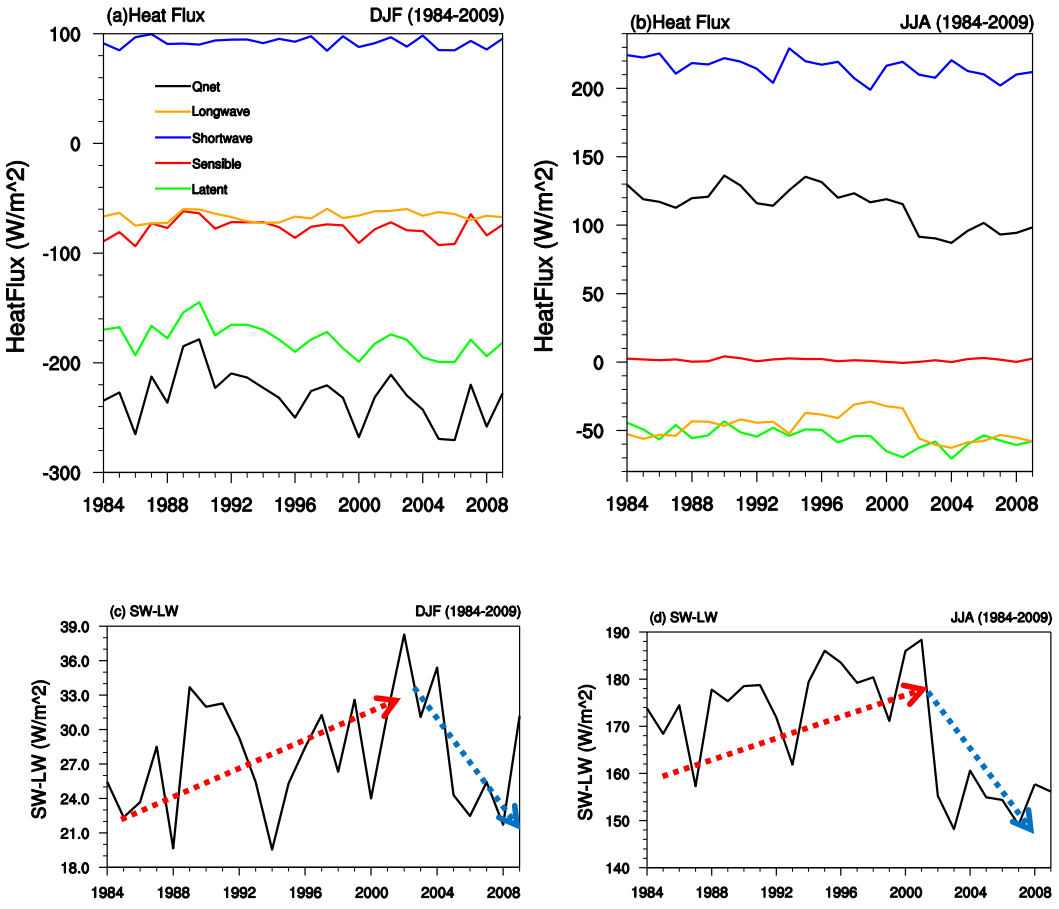

FIG. 11. Time series of (a),(b) net surface heat flux (black), net shortwave radiation (SW, blue), net longwave radiation (LW, orange), sensible heat (SH, red), and latent heat (LH, green) flux; (c),(d) net radiation during (a),(c) winter and (b),(d) summer over the East China Sea during 1984–2009. Positive (negative) values of SW, LW, SH, LH, total net surface heat flux, and net radiation flux (SW − LW) are defined as the ocean receiving (losing) heat from (to) the atmosphere. The red (blue) arrows in (c) and (d) indicate schematically the increase (decrease) of the net radiation flux. Data are from the ISCCP and OAFlux.

positive (negative) Q_{net} (Figs. 11 and 12) indicates that the ocean receives (loses) heat from (to) the atmosphere.

Figures 11a and 11b show that Q_{net} over the ECS is negative (positive) in winter (summer) during 1984–2009. Net radiative fluxes (RF) between net SW and net LW in winter and summer are positive, and, although they decreased slightly after 2001 and 2002 (Figs. 11c,d), they still contribute to SST increases in the ECS. As for the ECS, Fig. 12 presents the time series of yearly net SW, net LW, SH, LH, and Q_{net} during winter and summer for the SCS during 1984–2009. The Q_{net} and its changes are smaller than those for the ECS, but RF values for the SCS in both seasons are larger than those for the ECS, and contribute to SST increases. In addition, the change in LH has been mainly responsible for the changes in Q_{net} over the ECS since 1990 (Fig. 11). However, the changes in Q_{net} for the SCS are not as obvious as those for the ECS (Fig. 12).

It has been suggested that positive SST anomalies, particularly in extratropical regions such as the western boundary current of the North Pacific, favor vigorous turbulent heat release from the ocean to the atmosphere; specifically, decadal-scale SST anomalies (SSTAs) can force the overlying atmosphere (Tanimoto et al. 2003; Sugimoto and Hanawa 2011). For this reason, the relationship between SST and turbulent heat fluxes such as LH and SH is investigated and discussed for interdecadal time scales.

In a comparison of the changes in Q_{net} and its components, such as LH (Fig. 11), the positive relationship between SST and LH (figure not shown) indicates that increasing SST is responsible for the increase in Q_{net} from the ocean to the atmosphere due to an increase in upward LH flux since 1984. This implies that robust coastal warming has been forcing warming upon the atmosphere via the surface heat flux since the mid-1980s, similar to the

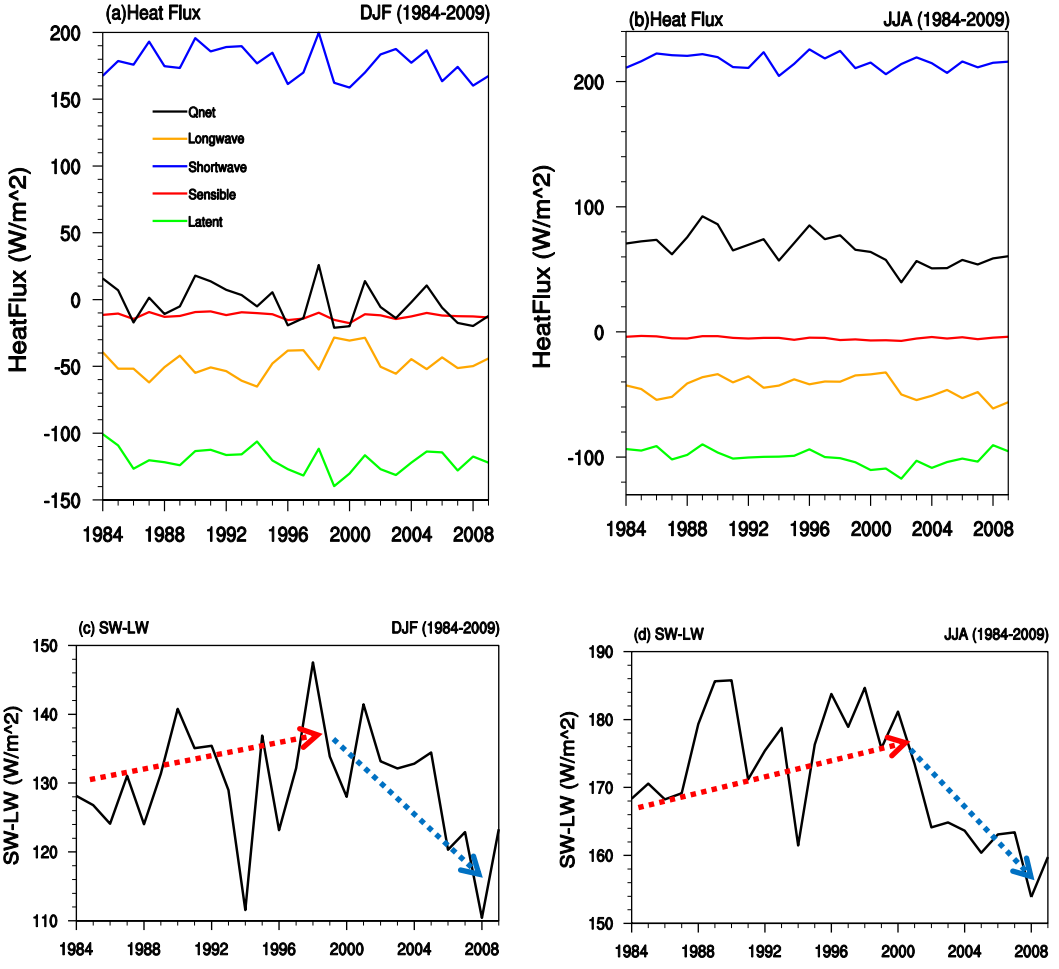

FIG. 12. As in Fig. 11, but for the South China Sea during 1984–2009. Data are from ISCCP and OAFlux.

results of Gulev et al. (2013), Sugimoto and Hanawa (2011), and Tanimoto et al. (2003). Therefore, it is suggested that the increase in absolute values of Q_{net} from the ocean to the atmosphere has a cooling feedback effect on SST. In summer, the positive correlation between SST and LH is similar to that in winter (figure not shown). However, summer LH and SH over the ECS are less than those in winter, and the RF in summer is much greater than in winter. This may explain why summer Q_{net} is positive and winter Q_{net} is negative, which have warming and cooling effects on SST, respectively.

d. *Relative contributions of oceanic heat transport and surface heat flux to surface warming*

Surface processes related to oceanic lateral advection, vertical entrainment, and surface heat flux can affect SST variability on interannual to interdecadal time scales. The previous analysis indicates that Q_{net} from the ocean to the atmosphere has increased since 1984 and has had a cooling effect on the sea surface in winter, despite the net radiative flux contribution to surface warming. In the following, therefore, we investigate the proportion of warming in offshore China during a weakening EAM period (i.e., for 1984–2008) (e.g., shown in Figs. 3a and 3b) based on available data, that is caused by oceanic lateral heat transport, vertical entrainment, and sea surface heat flux.

1) WINTER

To assess the relative importance of different processes on the seawater temperature anomaly tendency, the seawater temperature budget equation by Kang et al. (2001) and Foltz et al. (2003) is introduced:

$$\frac{\partial T'}{\partial t} = -\mathbf{V}\cdot\nabla T - \frac{T - T_{-h}}{h}w_e - \frac{1}{h}\nabla\cdot\int_{-h}^{0}\hat{v}\hat{T}dz + \frac{1}{\rho c_p h}Q'_{\text{net}}R, \quad (1)$$

where T' is the anomaly of the vertically averaged seawater temperature (T) in the upper mixed layer of

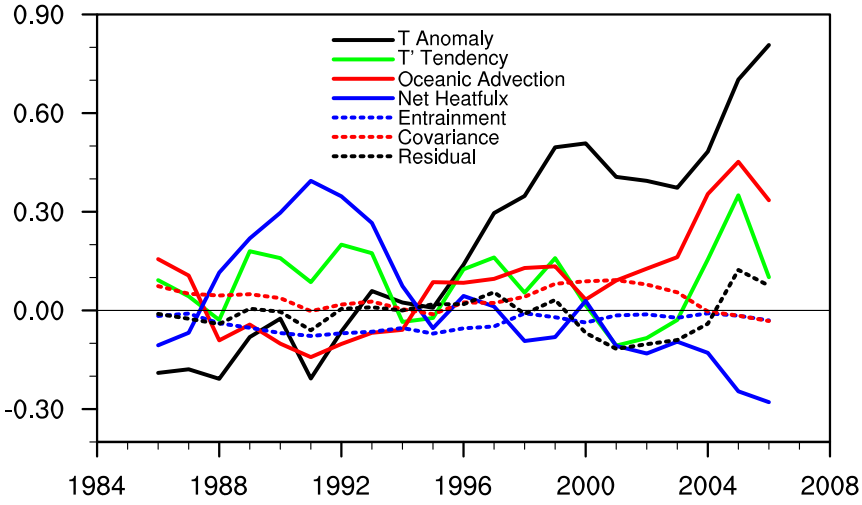

FIG. 13. Time series for the period 1984–2008 of the 5-yr running-mean winter values of the vertically integrated upper mixed layer temperature anomaly (black solid line) in °C; and temperature anomaly tendency (green solid line), vertical mixing entrainment (blue dotted line), vertical temperature–velocity covariance (red dotted line), net surface heat flux anomaly (blue solid line), and residual term (black dotted line) in °C month^{-1}. Data are from ISCCP and SODA.

varying depth (h); h is referred to as the depth at which the seasonal mean seawater temperature difference from the near-surface temperature (at 5 m in SODA) is 0.5°C for a given summer or winter; t is time; $\mathbf{V}$ is the horizontal velocity vector; w_e is the entrainment velocity, which can be written as $w_e = \partial h/\partial t + \nabla \cdot h\mathbf{V}$; T_{-h} is the temperature at the base of the variable depth mixed layer (h); $\hat{v}$ and $\hat{T}$ are the deviations from the vertically averaged horizontal velocity (v) and temperature (T), respectively (Stevenson and Niiler 1983); and R is a residual term. According to Eq. (1), the T' tendency ($\partial T/\partial t$) is affected by horizontal advection, vertical mixing entrainment, vertical temperature–velocity covariance, net surface heat flux anomaly (Q'_{net}), and residual terms (R). Here, $Q'_{\text{net}} = Q_{\text{net}} - Q_{-h}$, where Q_{net} is the same as that (Q_{net}) in Figs. 11 and 12, and Q_{-h} is the diffusive heat flux at the mixed layer depth (h), which is not estimated.

Figure 13 shows the 5-yr running mean wintertime series of all terms in Eq. (1), along with the temperature anomaly (T') for the period 1984–2008. We observe that the T' tendency term (green solid line) remains positive in most of the years, but the horizontal advection (red solid line) and net surface heat flux (Q'_{net}) (blue solid line) terms change from negative to positive and positive to negative, respectively, around 1994–95. In addition, the vertical entrainment term is weak, which seems to agree with the results obtained by Liu et al. (2014). This indicates that the oceanic lateral advection and net surface heat flux anomaly (Q'_{net}) terms have positive effects on the seawater temperature anomaly rising trend during different epochs, the former during the period after 1995 and the latter during the period 1988–95. It is also worth noting that the contribution of the oceanic lateral advection term to the positive T' trend gradually increased after 1995. The total contributions of ocean heat advection and net surface flux processes (Q'_{net}) to the robust warming over the ECS (22°–33°N, 120°–130°E) in winter for 1984–2000 are investigated by computing the time integral of the respective terms in Eq. (1). Here, the time integral of T' tendency values in the ECS shows that T' increased steadily by 1.75°C over that period. The total contributions of zonal and meridional ocean heat advection and Q'_{net} to T' are ~1.74° and ~0.42°C, respectively, for the entire period of 1984–2008 despite that the contribution of Q'_{net} to T' is basically negative since 1995 (Fig. 13). Hence, based on an observed persistent weakening of EAWM over the ECS since the late 1980, especially after 1995 (Figs. 3a and 3b) and associated change in ocean current (Fig. 4b), it is inferred that winter surface warming in the ECS during a weakening EAWM is mainly driven by oceanic lateral heat transport, with a secondary contribution from the Q'_{net}.

Figure 14 shows the zonal, meridional, and total heat advection regressed against the PC1 (EAWM) for 1958–2008. Oceanic lateral transport, especially meridional advection of the KC and its cross-shelf current toward the southern ECS and northern SCS, passively responds to a weakening EAWM (Figs. 14a and 14b), in which meridional advection is much more intense [by a factor of ~(2–3)] than zonal advection (Fig. 15). This may have contributed greatly to surface warming in the ECS and northern SCS during 1984–2008, which could be

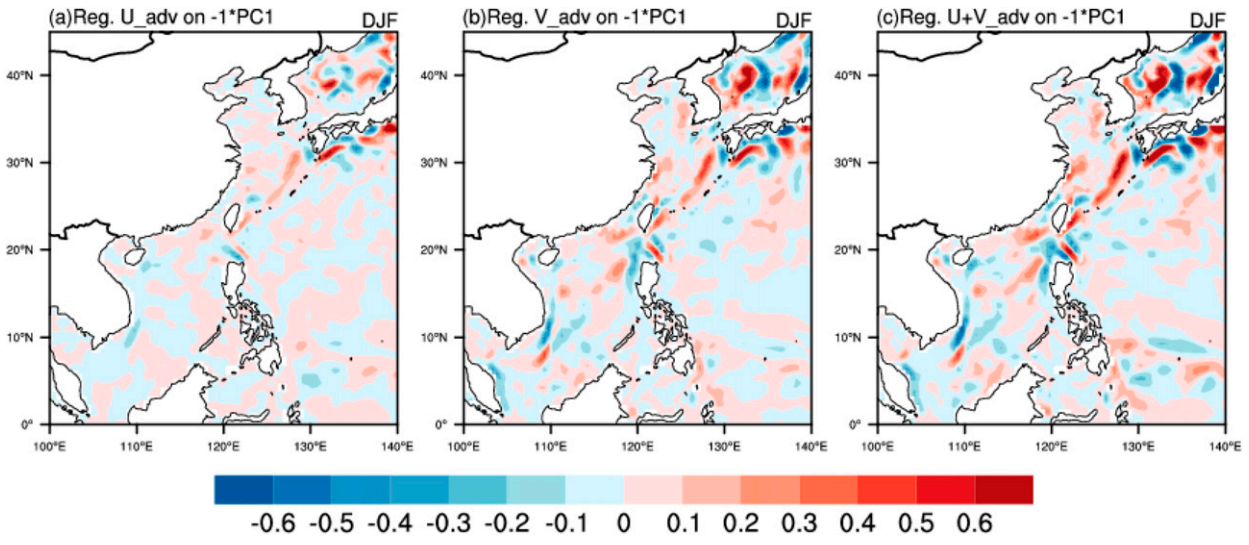

FIG. 14. Distributions of winter oceanic (a) zonal heat advection, (b) meridional heat advection, and (c) total horizontal heat advection regressed against the negative of the PC1 of the EAWM wind for 1958–2008. Data are from SODA and JRA-55.

explained by the regression pattern of currents against the PC1 (EAWM) in Figs. 3a and 4b. Moreover, a weakening southward YSCC from the YS caused by the weakening EAWM wind favors surface warming in the ECS (Fig. 4b).

2) SUMMER

Figure 15 indicates the 5-yr running mean summertime series for all terms in Eq. (1), along with the temperature anomaly (T') for the period 1984–2008. Summer T' in the ECS increased until 2002, when it declined notably. The total change in T' in the ECS, obtained by the time integral of the T' tendency values, was an increase of ~0.83°C during 1984–2002, with total contributions of oceanic lateral advection and Q'_{net} of −0.28° and 2.2°C, respectively, despite the positive to negative Q'_{net} changes in the early 2000s (Fig. 15). This indicates that the total contribution of summer Q'_{net} changes had a warming effect on the ECS during this period. However, the T' tendency, oceanic heat advection, and Q'_{net} terms all show a clear decreasing trend after 2002, with magnitudes of −0.72°, −0.21°, and −1.0°C, respectively. This may explain why summer T' had a sharper decline than that in winter (Figs. 13 and 15), which is similar to the results shown in Figs. 3c and 5c.

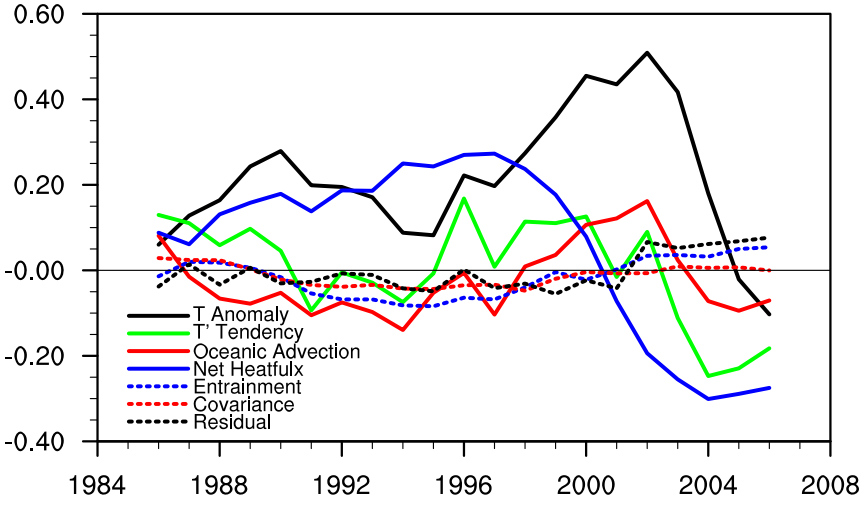

FIG. 15. As in Fig. 13, but for summer.

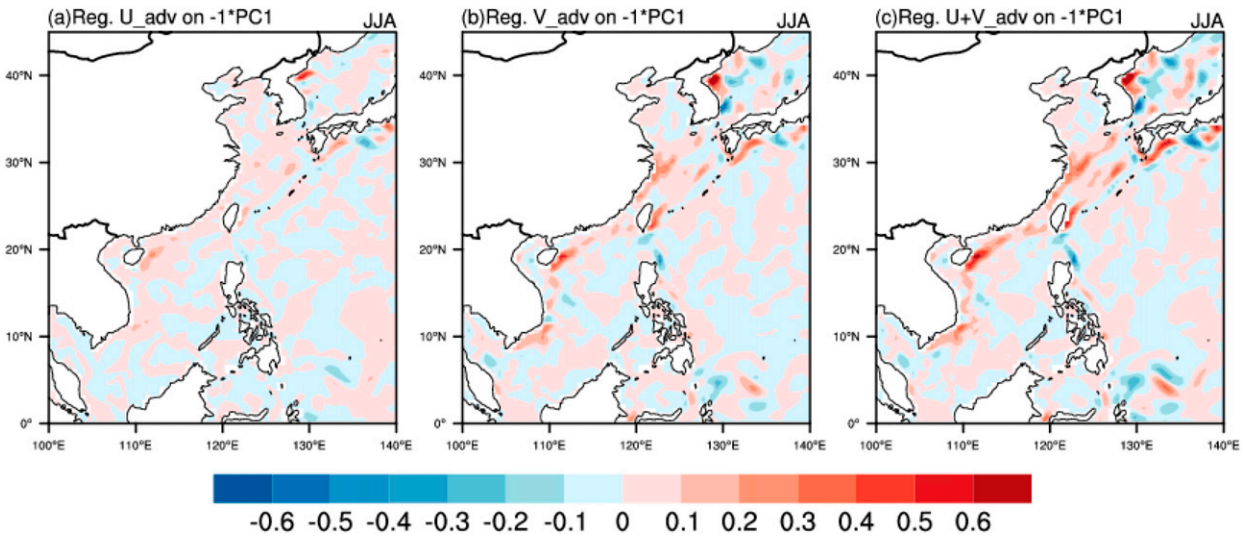

FIG. 16. As in Fig. 14, but for summer.

In addition, the regressed results of zonal and meridional heat advection against the PC1 (EASM) for 1958–2008 suggest that the interdecadal weakening of EOF1 EASM favors northward warming advection, with meridional advection being significantly larger than zonal advection, as in winter (Fig. 16). Strong meridional transport mainly results from the KC east of Taiwan Island and coastal currents in the northern SCS as well as on both sides of Taiwan. Enhanced northward heat contributes to surface warming in the ECS. It should be noted that our estimates of the principal drivers of coastal warming are preliminary and need further exploration.

4. Summary and conclusions

Over the past decades, robust surface warming with distinct interdecadal variations has been observed in offshore China during both winter and summer. The SST in offshore China (e.g., in the ECS region) during winter increased by ~1.71°C at a rate of 0.3° ± 0.04°C decade^{-1}, and by ~0.86°C at a rate of 0.15° ± 0.03°C decade^{-1} during summer. This indicates that SST warming rates have been greater than the mean warming rates of the global ocean since the 1980s.

On interdecadal time scales, robust surface warming in offshore China since the 1980s is negatively correlated with the weakening EOF1 EAM in winter and summer, but positively correlated with the strengthening EOF3 EASM anticyclone. The surface warming hiatus in offshore China after 1999 accompanied a slight rebound of the EOF1 EAM wind and the EOF3 EASM anticyclone. These results suggest that a weakening EOF1 EAWM contributed to winter surface warming in offshore China, particularly in the ECS region. This process proceeded via a strengthening of the intrusion of the KC branch and TWC into the ECS and a weakening of the cold YSCC. In the same period, a weakening EOF1 EASM enhanced the YSWC, contributing to summer surface warming in the northern ECS and YS, albeit not as strongly as in winter. Both the weakening EOF1s of EAWM and EASM could enhance KC flow into the SCS through the Luzon Strait, contributing to surface warming in the northern SCS. Additionally, the strengthening EOF3 EASM anticyclone (WPSH) in summer since the 1980s is responsible for increasing the flow of the KC branches into the ECS and SCS, and the TWC into the ECS, contributing to surface warming in the ECS and northern SCS by transporting heat from the KC.

An estimate of the contributions of oceanic heat advection, vertical entrainment, and surface heat flux suggests that the interdecadal variations of EAM forcing on SST are manifested by KC's lateral heat transfer, which can be attributed to Ekman advection effects. In addition to the effects of the EAM on SST through heat transfer by the KC, increasing atmospheric radiation, especially solar SW heat flux linked to the strengthening westward extension of the WPSH and consistent with the strengthening EOF3 EASM anticyclone since the 1980s, impacts surface warming in offshore China. Furthermore, the robust winter surface warming during 1984–2000 in the ECS can be largely attributed to increasing oceanic advection caused by weakening EAWM winds, although the increasing surface heat flux from the ocean to the atmosphere during winter has a

cooling feedback effect on offshore China. However, because of limited available data, it remains quantitatively unclear how much of the interdecadal SST variations in offshore China are influenced by a strengthening EAM, and how interdecadal changes in surface heat flux in turn alter SST. Therefore, additional research is required to explore the contributions of these various processes.

In addition, the datasets used in our study were compared to other datasets such as the ERA-40, the ERA-Interim, the NCEP–NCAR reanalysis, the China Ocean Reanalysis (CORA), and the Global Ocean Data Assimilation System (GODAS). However, the atmospheric and ocean reanalysis data, including wind, ocean currents, and surface heat fluxes used in this study still have uncertainties that should be reduced in future versions of these reanalysis datasets by taking advantage of future developments in measurement and reanalysis technologies.

Acknowledgments. We thank the anonymous reviewers and Editor Dr. Hisashi Nakamura for their constructive comments and suggestions. This research was supported by the National Key Research and Development Program of China (2017YFA0604902), the Grant China Clean Development Mechanism (CDM) Fund Project (2014112), China-Greece Bilateral Cooperation of Maritime Affairs, and the Chinese Special Scientific Research Project for Public Interest (201006021).

REFERENCES

Belkin, I. M., 2009: Rapid warming of large marine ecosystems. *Prog. Oceanogr.*, **81**, 207–213, doi:10.1016/j.pocean.2009.04.011.

Bjerknes, J., 1964: Atlantic air-sea interaction. *Advances in Geophysics*, Vol. 10, Academic Press, 1–82, doi:10.1016/S0065-2687(08)60005-9.

Cai, R. S., Q. L. Zhang, and Q. H. Qi, 2009: Spatial and temporal oscillation and long-term variation in sea surface temperature field of the South China Sea. *Chin. J. Oceanogr. Taiwan Strait*, **28** (4), 559–568.

——, J. L. Chen, and H. J. Tan, 2011: Variations of the sea surface temperature in the offshore area of China and their relationship with the East Asian monsoon under the global warming. *Chin. Climatic Environ. Res.*, **16** (1), 94–104.

——, J. P. Zhang, and Q. H. Qi, 2015: A study on the role of East Asian monsoon in variations of sea surface height in the East China Sea and its adjacent seas. *Chin. J. Appl. Oceanogr.*, **34** (2), 151–158.

——, H. J. Tan, and Q. H. Qi, 2016: Impacts of and adaptation to inter-decadal marine climate change in coastal China seas. *Int. J. Climatol.*, **36**, 3770–3780, doi:10.1002/joc.4591.

Carton, J. A., and B. S. Giese, 2008: A reanalysis of ocean climate using Simple Ocean Data Assimilation (SODA). *Mon. Wea. Rev.*, **136**, 2999–3017, doi:10.1175/2007MWR1978.1.

Chang, C. P., Y. Zhang, and T. Li, 2000: Interannual and interdecadal variations of the East Asian summer monsoon and tropical Pacific SSTs. Part I: Role of the subtropical ridge. *J. Climate*, **13**, 4310–4325, doi:10.1175/1520-0442(2000)013<4310:IAIVOT>2.0.CO;2.

Chang, Y. L., L. Y. Oey, C. R. Wu, and H. F. Lu, 2010: Why are there upwellings on the northern shelf of Taiwan under northeasterly winds? *J. Phys. Oceanogr.*, **40**, 1405–1417, doi:10.1175/2010JPO4348.1.

Chao, S. Y., 1991: Circulation of the East China Sea, a numerical study. *J. Oceanogr.*, **42**, 273–295.

Duchon, C. E., 1979: Lanczos filtering in one and two dimensions. *J. Appl. Meteor.*, **18**, 1016–1022, doi:10.1175/1520-0450(1979)018<1016:LFIOAT>2.0.CO;2.

Ebita, A., and Coauthors, 2011: The Japanese 55-year Reanalysis "JRA-55": An interim report. *Sci. Online Lett. Atmos.*, **7**, 149–152, doi:10.2151/sola.2011-038.

Foltz, G. R., S. A. Grodsky, J. A. Carton, and M. J. McPhaden, 2003: Seasonal mixed layer heat budget of the tropical Atlantic Ocean. *J. Geophys. Res.*, **108**, 3146, doi:10.1029/2002JC001584.

Gulev, S. K., M. Latif, N. Keenlyside, W. Park, and K. P. Koltermann, 2013: North Atlantic Ocean control on surface heat flux on multidecadal timescales. *Nature*, **499**, 464–467, doi:10.1038/nature12268.

Hoegh-Guldberg, O., R. S. Cai, E. S. Poloczanska, P. G. Brewer, S. Sundby, K. Hilmi, V. J. Fabry, and S. Jung, 2014: The ocean. *Climate Change 2014: Impacts, Adaptation, and Vulnerability. Part B: Regional Aspects*, V. R. Barros et al., Eds., Cambridge University Press, 1655–1731.

Hu, Z. Z., 1997: Interdecadal variability of summer climate over East Asia and its association with 500 hPa height and global sea surface temperature. *J. Geophys. Res.*, **102**, 19 403–19 412, doi:10.1029/97JD01052.

Jung, S., I. C. Pang, J. H. Lee, and H. K. I. Choi, 2014: Latitudinal shifts in the distribution of exploited fishes in Korean waters during the last 30 years: A consequence of climate change. *Rev. Fish Biol. Fish.*, **24**, 443–462, doi:10.1007/s11160-013-9310-1.

Kalnay, E., and Coauthors, 1996: The NCEP/NCAR 40-Year Reanalysis Project. *Bull. Amer. Meteor. Soc.*, **77**, 437–471, doi:10.1175/1520-0477(1996)077<0437:TNYRP>2.0.CO;2.

Kang, I. S., I. S. An, and F. F. Jin, 2001: A systematic approximation of the SST anomaly equation for ENSO. *J. Meteor. Soc. Japan*, **79**, 1–10, doi:10.2151/jmsj.79.1.

Liu, N., D. Wu, X. Lin, and Q. Men, 2014: Seasonal variations of air–sea heat fluxes and sea-surface temperature in the northwestern Pacific marginal seas. *Acta Oceanol. Sin.*, **33**, 101–110, doi:10.1007/s13131-014-0433-6.

Mu, Q. Z., S. W. Wang, J. H. Zhu, and D. Y. Gong, 2001: Variations of the Western Pacific Subtropical High in summer during the last hundred years. *Chin. J. Atmos. Sci.*, **25** (6), 787–797.

Oey, L. Y., M. C. Chang, Y. L. Chang, Y. C. Lin, and F. H. Xu, 2013: Decadal warming of coastal China Seas and coupling with winter monsoon and currents. *Geophys. Res. Lett.*, **40**, 6288–6292, doi:10.1002/2013GL058202.

——, Y. L. Chang, Y. C. Lin, M. C. Chang, S. Varlamov, and Y. Miyazawa, 2014: Cross flows in the Taiwan Strait in winter. *J. Phys. Oceanogr.*, **44**, 801–817, doi:10.1175/JPO-D-13-0128.1.

Qi, Q. H., R. S. Cai, and Q. L. Zhang, 2010: Low-frequency variability of the heat transport in source area of Kuroshio and its relation to SST in China seas. *Chin. J. Oceanogr. Taiwan Strait*, **29** (1), 106–113.

Rayner, N. A., D. E. Parker, E. B. Horton, C. K. Folland, L. V. Alexander, D. P. Rowell, E. C. Kent, and A. Kaplan, 2003: Global analyses of sea surface temperature, sea ice, and night

marine air temperature since the late nineteenth century. *J. Geophys. Res.*, **108**, 4407, doi:10.1029/2002JD002670.

Rhein, M., and Coauthors, 2013: Observations: Ocean. *Climate Change 2013: The Physical Science Basis*, T. F. Stocker et al., Eds., Cambridge University Press, 255–315.

Sherman, K., I. M. Belkin, K. D. Friedland J. O'Reilly, and K. Hyde, 2009: Accelerated warming and emergent trends in fisheries biomass yields of the world's large marine ecosystems. *Ambio*, **38**, 215–224, doi:10.1579/0044-7447-38.4.215.

Stevenson, J. W., and P. P. Niiler, 1983: Upper ocean heat budget during the Hawaii-to-Tahiti shuttle experiment. *J. Phys. Oceanogr.*, **13**, 1894–1907, doi:10.1175/1520-0485(1983)013<1894:UOHBDT>2.0.CO;2.

Sugimoto, S., and K. Hanawa, 2011: Roles of SST anomalies on the wintertime turbulent heat fluxes in the Kuroshio Oyashio confluence region: Influences of warm eddies detached from the Kuroshio extension. *J. Climate*, **24**, 6551–6561, doi:10.1175/2011JCLI4023.1.

Tanimoto, Y., H. Nakamura, T. Kagimoto, and S. Yamane, 2003: An active role of extratropical sea surface temperature anomalies in determining anomalous turbulent heat flux. *J. Geophys. Res.*, **108**, 763–765, doi:10.1029/2002JC001750.

Tian, Y. J., H. Kidokoro, T. Watanabe, Y. Igeta, H. Sakaji, and S. Ino, 2012: Response of yellowtail, *Seriola quinqueradiata*, a key large predatory fish in the Japan Sea, to sea water temperature over the last century and potential effects of global warming. *J. Mar. Syst.*, **91**, 1–10, doi:10.1016/j.jmarsys.2011.09.002.

Trenberth, K. E., 1984: Signal versus noise in the Southern Oscillation. *Mon. Wea. Rev.*, **112**, 326–332, doi:10.1175/1520-0493(1984)112<0326:SVNITS>2.0.CO;2.

——, and Coauthors, 2007: Observations: Surface and atmospheric climate change. *Climate Change 2007: The Physical Science Basis*, S. Solomon et al., Eds., Cambridge University Press, 235–336.

Wang, B., 1992: The vertical structure and development of the ENSO anomaly mode during 1979–1989. *J. Atmos. Sci.*, **49**, 698–712, doi:10.1175/1520-0469(1992)049<0698:TVSADO>2.0.CO;2.

Wang, L., and W. Chen, 2014: The East Asian winter monsoon: Re-amplification in the mid-2000s. *Chin. Sci. Bull.*, **59**, 430–436, doi:10.1007/s11434-013-0029-0.

Wu, L., and Coauthors, 2012: Enhanced warming over the global subtropical western boundary currents. *Nat. Climate Change*, **2**, 161–166, doi:10.1038/nclimate1353.

Yeh, S. W., and C. H. Kim, 2010: Recent warming in the Yellow/East China Sea during winter and the associated atmospheric circulation. *Cont. Shelf Res.*, **30**, 1428–1434, doi:10.1016/j.csr.2010.05.002.

Yuan, D., and Y. Hsueh, 2010: Dynamics of the cross-shelf circulation in the Yellow and East China Seas in winter. *Deep-Sea Res. II*, **57**, 1745–1761, doi:10.1016/j.dsr2.2010.04.002.

Zhang, Q., Y. J. Hou, and T. Z. Yan, 2012: Inter-annual and inter-decadal variability of Kuroshio heat transport in the East China Sea. *Int. J. Climatol.*, **32**, 481–488, doi:10.1002/joc.2295.

Zhang, R. H., 2015: Changes in East Asian summer monsoon and summer rainfall over eastern China during recent decades. *Sci. Bull.*, **60**, 1222–1224, doi:10.1007/s11434-015-0824-x.

Zheng, Q., G. Fang, and Y. T. Song, 2006: Introduction to special section: Dynamics and Circulation of the Yellow, East, and South China Seas. *J. Geophys. Res.*, **111**, C11S01, doi:10.1029/2005JC003261.

Zhou, T., and Coauthors, 2009: Why the western Pacific subtropical high has extended westward since the late 1970s. *J. Climate*, **22**, 2199–2215, doi:10.1175/2008JCLI2527.1.

Zhu, J. L., H. Liao, and J. P. Li, 2012: Increases in aerosol concentrations over eastern China due to the decadal-scale weakening of the East Asian summer monsoon. *Geophys. Res. Lett.*, **39**, L09809, doi:10.1029/2012GL053053.